Schreurs, G. and Colletta, B. 2002. Analogue modelling of continental transpression. In: Schellart , W. P. and Passchier, C. W. 2002. Analogue modelling of large-scale tectonic processes. Journal of the Virtual Explorer, 7, 67-80.

Analogue modelling of continental transpression

G. SCHREURS[1] & B. COLLETTA[2]

[1] *Institute of Geological Sciences, University of Bern, Baltzerstrasse 1, CH-3012 Bern, Switzerland*
schreurs@geo.unibe.ch, www.geo.unibe.ch/people/schreurs/main.htm
[2] *Institute Français du Pétrole, Division Géologie-Géochimie,*
92506 Rueil-Malmaison Cedex, France

Abstract: Experiments were performed to simulate deformation in zones of continental transpression. Stratified models consisted of brittle analogue materials overlying a thin layer of viscous material. Transpression was obtained by combining basal, distributed strike-slip shear with transverse shortening. Analysis of our models by X-ray computerized tomography allowed a detailed analysis of their internal geometry and kinematics. On the basis of X-ray CT images, short movies were generated using computer visualisation software.
The applied ratio of shear strain rate and shortening strain rate exerts an important control on initial fault evolution. In those experiments with a relatively high strain rate ratio (≥3.6), sub-vertical, en echelon strike-slip faults formed first, striking at angles of 25°-37° to the shear direction. During increasing deformation, several convergent strike-slip fault zones formed displaying positive flower structures. In contrast, failure of brittle layers in low strain rate ratio (≤2.7) experiments was accommodated by gently dipping (30-45°), downward converging thrust faults that bound pop-up structures and strike parallel to the shear direction. Although initially transpression is taken up either by pure strike-slip faults or by pure reverse faults, increasing deformation results in a fault pattern dominated by oblique-slip faults. Partial partitioning of fault motion occurred at late stages of transpression when strike-slip faults formed within pop-up structures. These strike-slip faults merge at depth with confining oblique-slip reverse faults, have a curved fault trace in plan view and a dip direction which changes along strike. Fault patterns can be used as kinematic indicators to determine whether transpression has a sinistral or dextral shear component. The detailed 3D imaging of our experiments might provide constraints for geometric and kinematic interpretations of complex structures in zones of continental transpression.

Introduction

Tectonic plates often converge obliquely and major regional structures have been interpreted as the result of oblique shortening (transpression). Examples are the Alpine Fault zone in New Zealand (Norris et al., 1990), the San Andreas Fault zone in central California (Mount & Suppe, 1987), the Mongolian Western Altai (Cunningham et al., 1996) and the Venezuela Andes (Colletta et al., 1997). Transpression in the upper crust is dominantly accommodated by brittle faulting and is generally thought to be at least partly controlled by distributed flow of the underlying ductile parts of the crust and mantle (England, 1989).

We performed a series of analogue modelling experiments to investigate the development and evolution of structures in zones of continental transpression. Models were analysed by X-ray computerized tomography (CT; Hounsfield, 1973), a technique which makes it possible to visualise the interior of a model without destroying it. Some of the experimental results have been previously published, illustrated with surface views, and CT images through selected stages of the model evolution (Schreurs & Colletta, 1998). In this paper emphasis is placed on computer animations of these experiments, which show in considerably more detail the development and evolution of transpressional structures.

Experimental set-up

Models were deformed in the experimental apparatus shown in Fig. 1. Transpression consisted of two components: a shear component at the base of the model (in a direction parallel to the longitudinal vertical walls) and a transverse shortening component (perpendicular to the longitudinal vertical walls). The base of the deformation box consisted of two plates (Fig. 1B). One of them was moved past the other by a geared motor drive. Some 60 plexiglass bars, each 5 mm wide, 1 cm high, and 70 cm long, were stacked like cards between two parallel wooden bars, which are attached to the base plates. The plexiglass bars were transversally confined on either side by a pivoting wooden bar. A 5 mm thin layer of viscous polydimethylsiloxane (PDMS; Weijermars, 1986) was placed on the array of plexiglass bars, and sand and glass powder (with an average grain size of 100 μm) were alternately poured on top to produce a stratified model (total thickness 3.5 cm). A square grid of colored sand markers was traced on the upper surface. Initial length of the model was 70 cm and initial width was 26 cm. Transverse borders of the model consisted of rubber sheets. As one of the base plates was displaced, the plexiglass bars slipped past one another and the initial rectangular configuration became a parallelogram and caused the shear component of deformation in the overlying model. At the same time

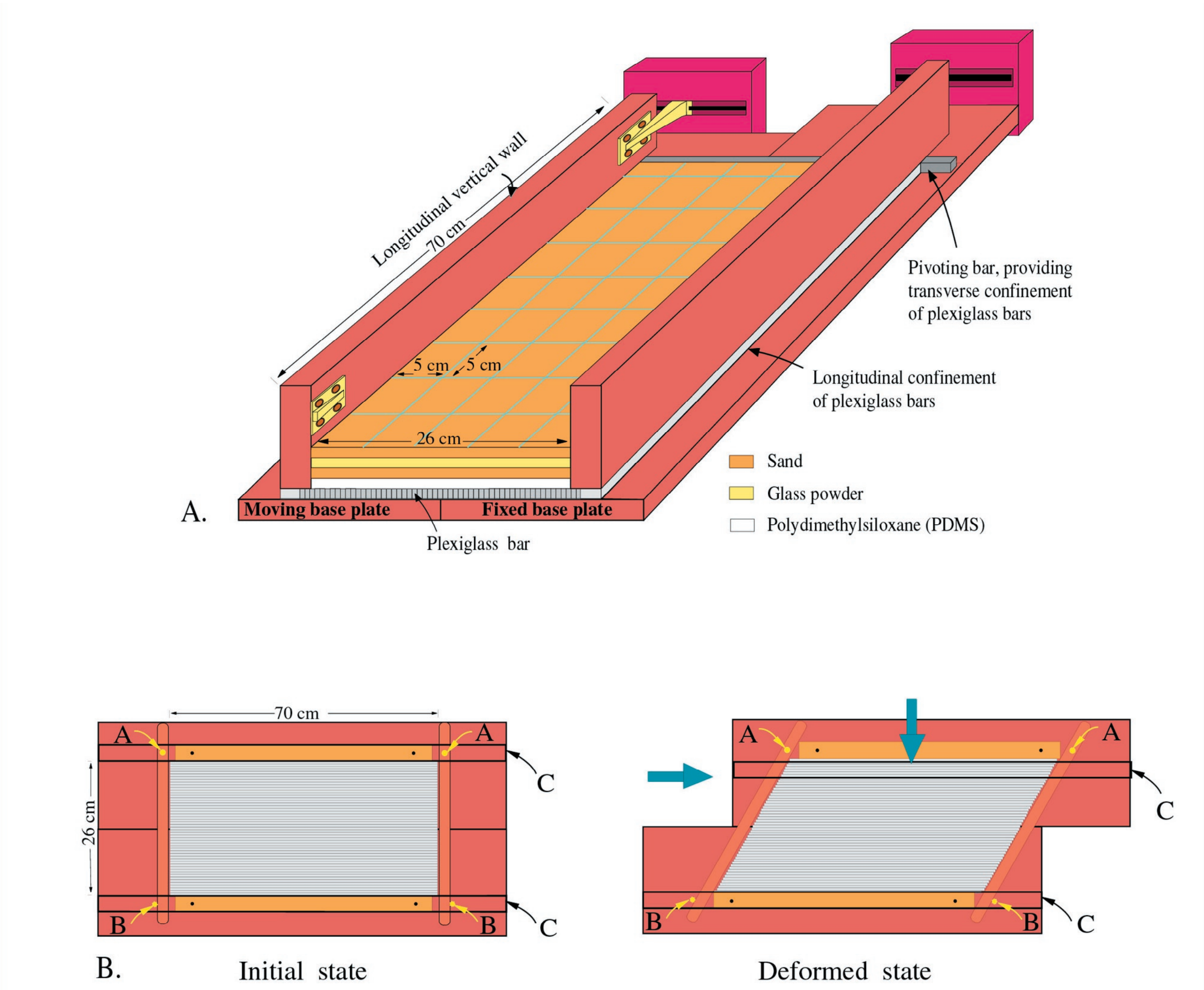

Figure 1. (A) Perspective view of experimentsal apparatus. Transverse borders of the multilayer model consisting of rubber sheets are not shown. (B) Plan view of base of experimental apparatus. Longitudinal vertical sidewalls, whose outline is marked by C, overlie the plexiglass bars. Transverse movement of one of these walls induced the shortening component of transpression. A and B indicate location of small pins that guide the pivoting wooden bars.

Experiment number	**1661**	**1764**	**1820**	**1770**
Duration of experiment (minutes)	132	170	200	240
Velocity of base plate (cm/h) (dextral shear component)	8	4	3	2
Total movement of base plate (cm)	17.6	11.3	10.0	8.0
Maximum shear strain (γ)	0.62	0.40	0.35	0.28
Shear strain rate ($10^{-5}s^{-1}$)	7.8	3.9	2.9	1.9
Transverse shortening velocity (cm/h)	1	1	1	1
Final width of model (initial width 26 cm)	23.8	23.2	22.7	22.0
Maximum shortening (in %)	8.5	10.9	12.8	15.3
Shortening strain rate ($10^{-5}s^{-1}$)	1.07	1.07	1.07	1.07
Strain rate ratio (ratio of shear strain rate and shortening strain rate)	7.3	3.6	2.7	1.8

Table 1. Experimental parameters. Shear strain and shear strain rate were calculated using the width of the array of plexiglass bars (28.5 cm), which was slightly larger than the initial width of the overlying model (26 cm). Model widths were used to calculate shortening and shortening strain rate.

transverse shortening was produced by displacement of one of the longitudinal vertical walls (C in Fig. 1b), which overlie both the array of plexiglass bars and their two confining pivoting wooden bars. The viscous PDMS at the base of the model served two purposes: it distributed the applied shear movement homogeneously and at the same time it simulated a horizontal detachment layer, because it was weaker than the overlying sand and glass powder. Movements of both longitudinal vertical wall and base plate occurred at pre-set velocities by stepper motors with computer control.

Most previous studies on oblique shortening involved a single basal discontinuity for the shear component of deformation, causing localisation of structures in the immediate vicinity of the discontinuity. This is in contrast with the experiments shown here, in which the shear component of deformation is distributed, resulting in the development of several fault zones and thus allowing to study their interactions. The boundary conditions for four transpressional experiments (Table 1) were identical, except for the velocity of the base plate which induced the dextral shear component of transpression, hence the ratio between shear strain rate and shortening strain rate. Varying this parameter between experiments allowed us to investigate its influence on fault development in the brittle layers.

Experiments

The experiments are described in order of decreasing strain rate ratio. The structures in each model are documented by line drawings, surface photographs, CT images and short movies. During deformation of the model a series of vertical sections perpendicular to the longitudinal sidewalls were obtained at regular time intervals using the X-ray technique. At the end of each experiment 135 closely spaced serial cross-sectional CT images were acquired. Plan view photographs of the model were also taken at regular time intervals and document the surface evolution. Visualisation software packages such as NIH Image©, Noesys T3D© and Adobe Photoshop©, were used to digitally enhance CT images, and to compute both horizontal sections and 3D perspective views of the final deformation stage. Surface photographs and enhanced CT images were used to create short movies. These include movies of the surface evolution, movies of the temporal evolution of structures in vertical sections perpendicular to the shear direction, movies of serial 2D cross-sections and 3D perspective views of the final stage of transpression.

Experiment 1661 (strain rate ratio 7.3)

At early stages of deformation two separate zones of en-echelon dextral strike-slip faults form in the brittle layers; (Fig 2A,B; Movies 1661-01, 1661-02) individual fault segments strike at angles between 24° and 30° with respect to the longitudinal borders. The early faults are important kinematic indicators: left-stepping faults in each zone indicate a dextral shear component. Faults are sub-vertical and extend down to the base of the brittle layers. Domains of positive vertical relief are created in areas where two adjacent left-stepping faults overlap. With increasing deformation individual fault segments propagated sideways with different strike orientations and dips. They acquire a slight sigmoidal trace (Z shaped; Fig. 2C) and a small reverse component, whose sense of dip changes along strike: for example, the hanging wall of fault X in section A becomes the footwall in section C (Fig. 2D), a characteristic of so-called scissor faults. With increasing deformation lower-angle dextral faults striking at 15° to 0° (Rl in Fig. 2E, with lower surface strikes than first-formed dextral faults) formed in the overlap area between adjacent left-stepping faults and linked with older faults. This led to an overall fault pattern dominated by major anastomosing dextral strike-slip fault zones. Between these fault zones several sinistral faults striking at high angles of 65° to 70° (R'l in Fig. 2E) developed. These secondary, antithetic faults accommodated only minor displacement and were generally confined between older major dextral fault zones. During increasing deformation, transpression was absorbed on several steeply dipping oblique-slip fault zones with an overall surface strike of about 15°. Movies 1661-03 and 1661-04 show vertical and horizontal serial sections, respectively, through these fault zones. These fault zones are similar to positive flower structures and characteristic of convergent strike-slip fault zone (Movies 1661-05 and 1661-06). The strike-slip component along the oblique-slip faults dominates over the reverse dip-slip component. In plan view dominant offset of faults is dextral, whereas in vertical sections they have a small reverse dip-slip component. Younger lower-angle dextral fault (Rl) branch at depth with older faults. Reverse faults forming at late stages of deformation near the acute borders of the sheared sand pack are boundary effects caused by "scissoring" of the model (Fig. 2E).

Experiment 1764 (strain rate ratio 3.6)

As in the previous experiment dextral strike-slip faults formed early (Fig. 3A,B; Movie 1764-01, 1764-02). The faults are again arranged en-echelon pattern and are left-stepping. However, their surface strike is now more oblique (between 28° and 37)° and reflects the decreasing strain rate ratio. With increasing deformation upward bulging of material occurred between overlapping strike-slip faults and faults obtained a reverse component of slip. Gently-dipping reverse faults, dipping 30-50° (e.g. fault Q in Fig 3C,D), formed in the center of the model between steep dextral convergent fault zones. These faults are interpreted to result from local stress field changes where the maximum compressive stress was reoriented sub-parallel to older strike-slip fault zones. The fact that low-angle reverse faults rather than strike-slip faults developed indicate that the intermediate principal stress axis switched locally from vertical to horizontal.

The lower half of Fig. 3E,F illustrates how strain was partitioned into predominantly pure strike-slip and predominantly pure shortening. Here strike-slip faults strike sub-parallel to gently dipping reverse faults that converge at depth to form a pop-up structure. The strike-

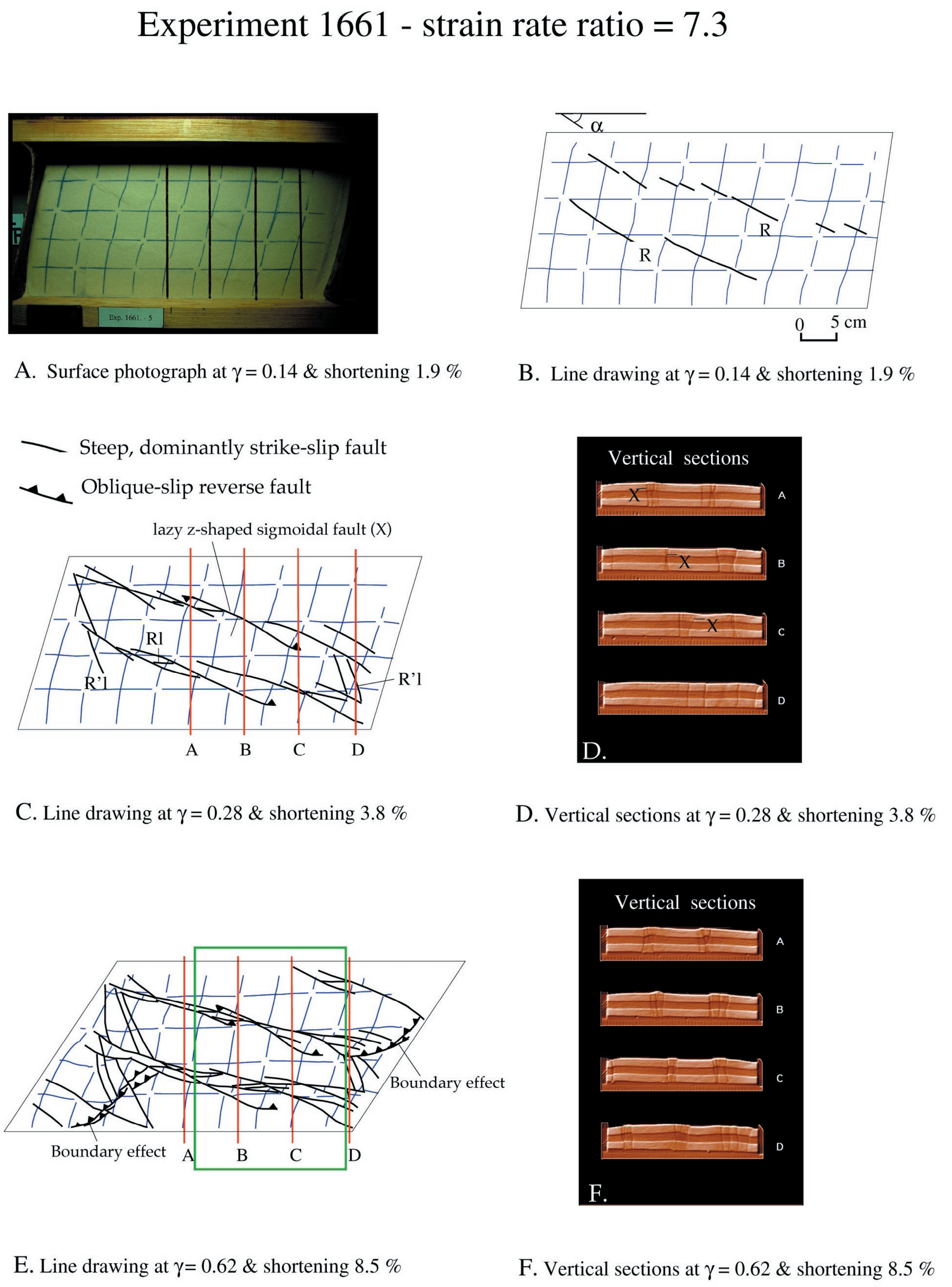

Figure 2. Transpression experiment 1661. (A) Plan view of early stage of transpression. (B,C,E) Line drawings after photographs illustrate fault evolution at three consecutive stages of transpression; fine lines represent coloured sand markers (initially square grids); bold lines represent traces of visible faults. R, in synthetic, dextral strike-slip fault (Riedel shear); R'l lower-angle antithetic fault; Rl, lower-angle synthetic fault. X in (C,D) marks location of scissor fault. Rectangle in (E) indicates area analysed by X-ray computerized tomography (D, F). Vertical sections showing fault evolution at two consecutive stages. Location of sections is indicated by A-D in corresponding line drawings.

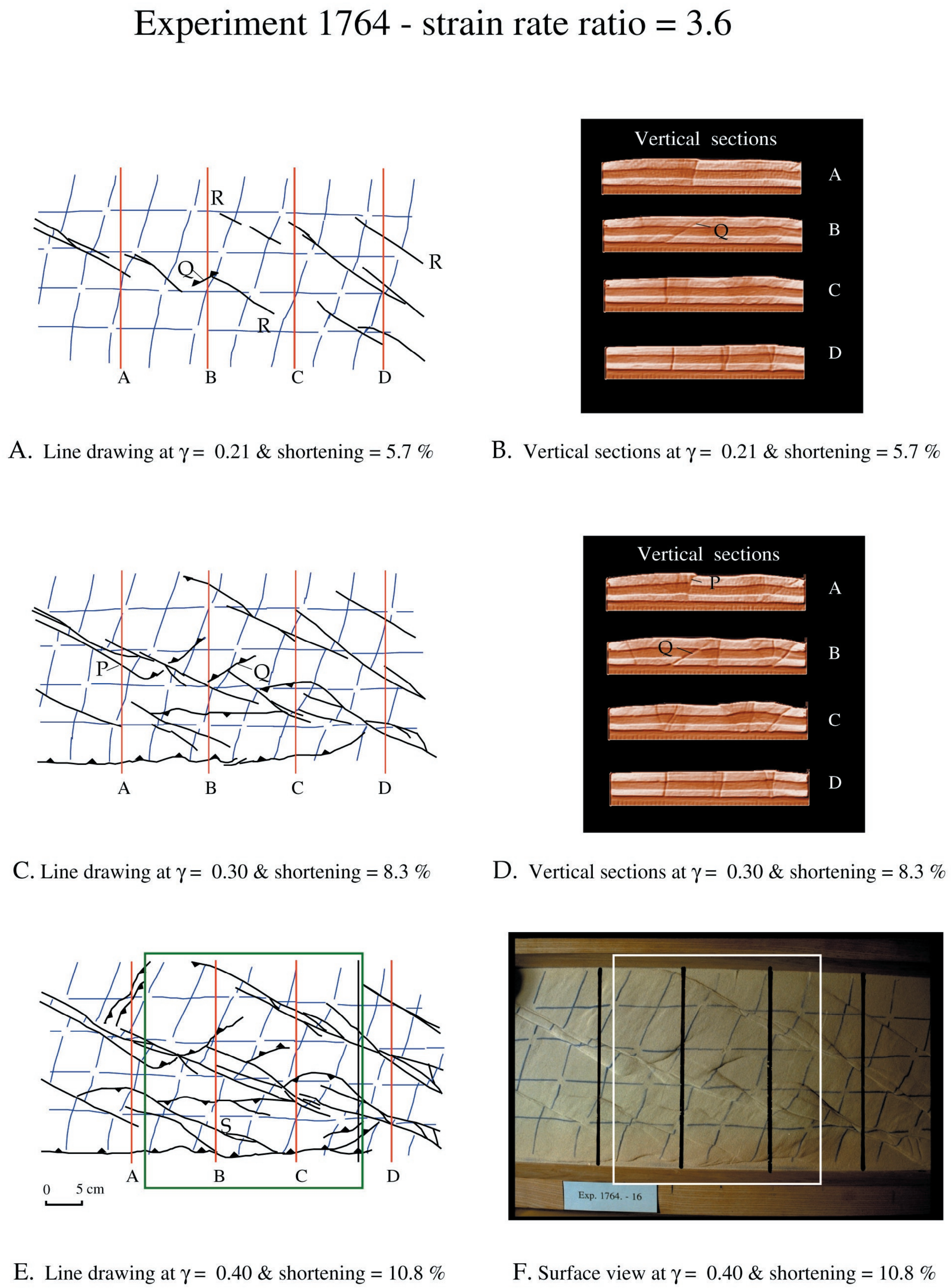

Figure 3. Transpression experiment 1764. (A,C,E) Line drawings after photographs illustrate fault evolution at three consecutive stages of transpression. R, synthetic, dextral strike-slip fault (Reidel shear). Faults P, Q and S are explained in text. (B,D) Vertical sections showing fault evolution at two consecutive stages. Location of sections is indicated by A-D in corresponding line drawings. (F) Surface view at final stage of transpression. Rectangle in (E,F) indicates area analysed by X-ray computerized tomography.

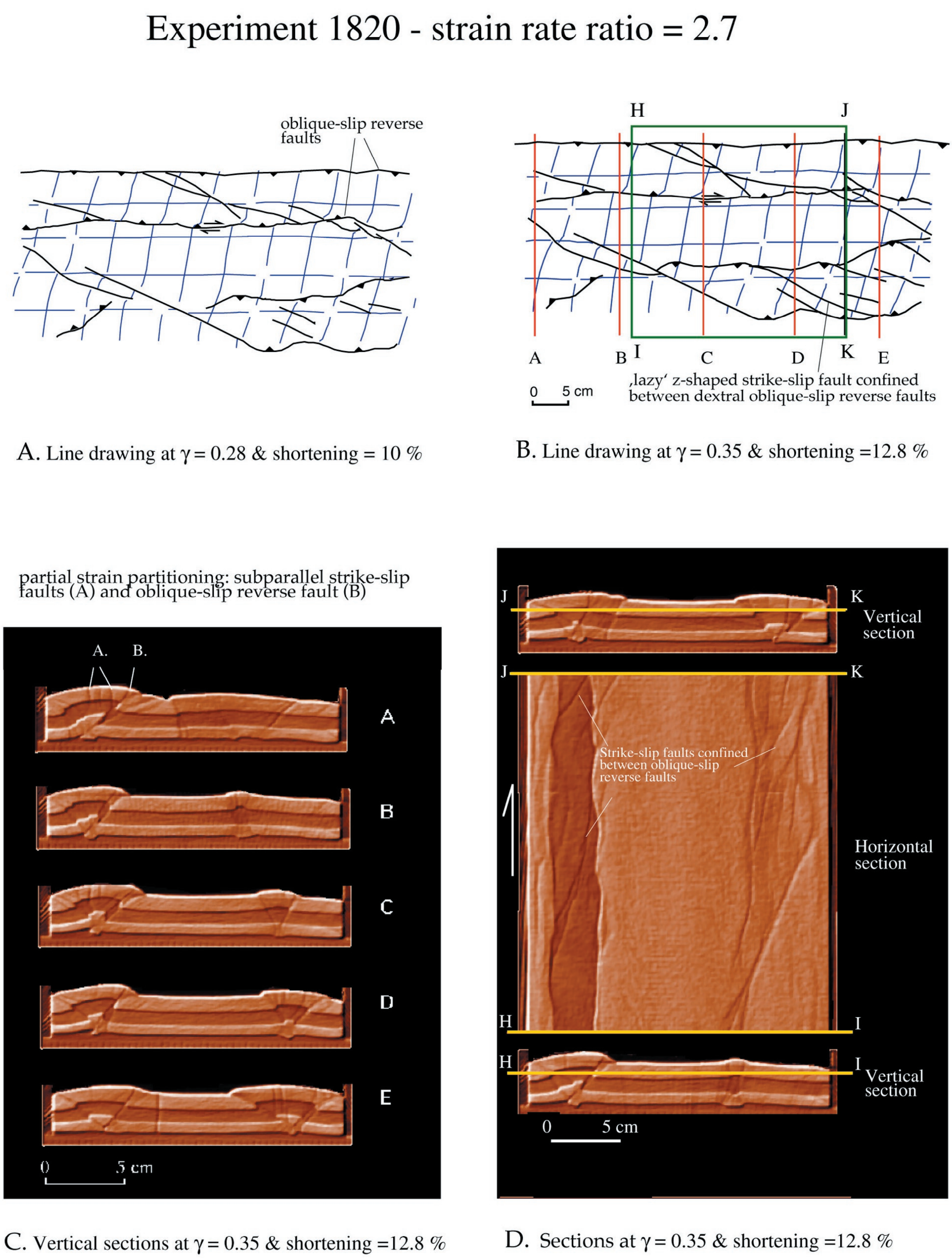

Figure 4. Transpression experiment 1820. (A,B) Line drawings after photographs document structural evolution at two consecutive stages of transpression; Rectangle HIJK indicates area analysed by X-ray computerized tomography. (C) Vertical sections showing fault evolution at final stage of transpression. Location of sections is indicated by A-E in (B), (D) Horizontal section at depth and vertical sections through final stage.

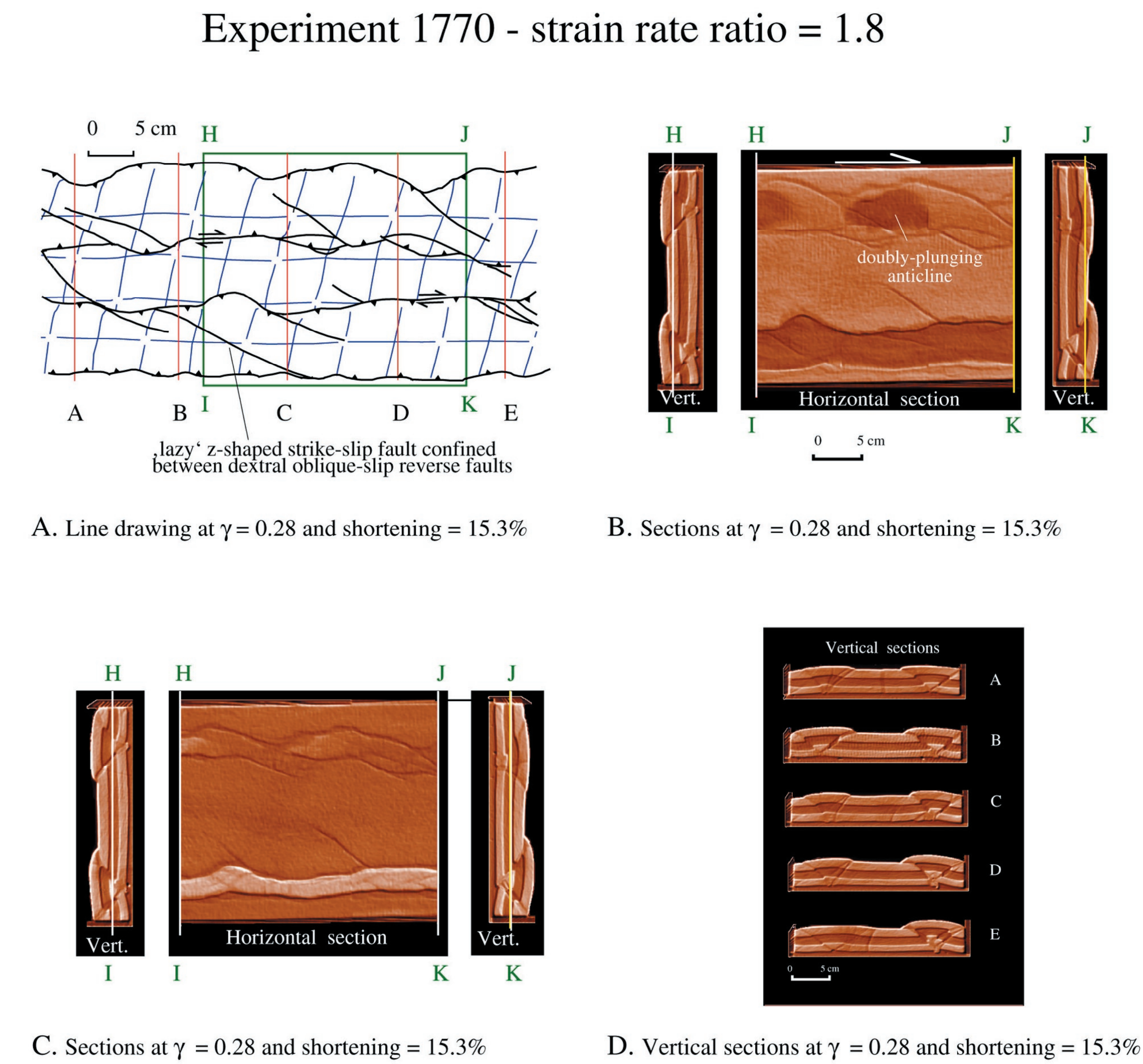

Figure 5. Transpression experiment 1770. (A) Line drawings after photograph illustrating fault pattern at final stage of transpression. Rectangle HIJK indicates area analysed by X-ray computerized tomography. (B,C) Horizontal section at depth and vertical sections through final stage. (D) Vertical sections showing fault evolution. Location of sections in indicated in (A).

slip faults dip steep at the surface and merge at depth with the bounding dominantly reverse faults (Movies 1764-03 and 1764-05). Fault dip can vary considerably along strike. Horizontal sections show the complex fault pattern at depth (Movie 1764-04). The fault zones narrow at depth, where strike-slip faults become sub-parallel to reverse faults.

Experiment 1820 (strain rate ratio 2.7)

Unlike in the previous two experiments, early transpression was taken up by reverse faulting rather than strike-slip faulting (Fig. 4A; Movies 1820-01, 1820-02). Thrust faults dipped at 35-45°, had opposite vergence and bounded a pop-up structure striking parallel to the longitudinal walls. The forward directed thrust predominantly accommodated further deformation and displayed a dextral strike-slip component (Fig. 4B). Dextral strike-slip faults formed within the pop-up structure (Fig. 4C, D). These faults are sub-vertical near the surface, but generally curved at depth and merged with older faults. In front of the pop-up structure a second pop-up structure and steeply dipping strike-slip faults formed. These structures interfered laterally and as a consequence the fault dip varied considerably along strike: from about 30° to sub-vertical (cf. sections B-E in Fig. 4C,D; Movies 1820-03, 1820-04 and 1820-05). Dextral strike-slip faults formed also within the second pop-up structure, striking at 15-25° (Movies 1820-03 and 1820-05). In this area we thus have a partitioning of fault motion between sub-parallel nearly pure strike-slip faults and nearly pure reverse dip-slip faults.

Experiment 1770 (strain rate ratio 1.8)

The evolution of this experiment is very similar to that of the previous one. At early stages of transpression a pop-up structure formed striking parallel to the longitudinal walls (Movie 1770-01). The dip of downward converging reverse faults was initially about 35° (Movie 1770-02). With increasing deformation they became dextral oblique-slip reverse faults. A second pop-up formed in front of the older one and also showed a strike-slip component Dextral strike-slip faults (striking at about 25°) formed within the pop-up structures (Movie 1770-02). They have a curved shape in plan view and coalesce with reverse faults (Fig. 4A,B). Some strike-slip faults formed in between pop-up structures (Fig. 5A-C). Vertical sections through the final stage of deformation (Fig. 5D; Movie 1770-03) clearly show the two pop-up structures. Late strike-slip faults within pop-up domains are sub-vertical near the upper surface but curve at depth and merge with oblique-slip reverse faults. In the case where a steep strike-slip fault branches at depth with both forward and backward directed oblique-slip reverse faults of a pop-up structure, its dip direction changes along strike. Horizontal sections reveal a doubly plunging anticline (upper part of fig. 5B; Movie 1770-04): the hinge zone defined by bulging layers in the pop-up domain changed its plunge direction laterally. The structure is partly bounded and partly cut by dextral strike-slip faults, which coalesce with major oblique-slip reverse faults (Movie 1770-05).

Discussion and conclusions

Anderson (1951) proposed that failure of homogeneous brittle material at a horizontal free surface should occur by reverse, normal or strike-slip faulting, but not by oblique-slip faulting. At depth, however, the orientation of principal stress axes need not necessarily be vertical or horizontal, and oblique-slip faulting might be possible. In our transpression experiments, initial failure in brittle layers is taken up by either nearly pure strike-slip faults or nearly pure thrust faults. This indicates that principal stresses throughout our model initially lie within sub-horizontal and sub-vertical planes. This implies that the thin layer of PDMS at the base of the model effectively decoupled the sand from the plexiglass bars and reduces the basal drag exerted on the sand by the plexiglass bars. Thus, in our models the basal shear stresses are considered to be negligible. Therefore, Anderson's theory seems appropriate for initial faulting in our experiments, which occurs in response to a stress field in which one principal stress direction is vertical and the two others lie within a sub-horizontal plane. Depending on the strain rate ratio, initial faults in as yet unfaulted granular material will be generated either as pure strike-slip faults or pure thrust faults. Once major faults have formed, however, the sand-glass powder cake consists of competent unfaulted material and incompetent dilatant fault zones. Additional deformation will then mostly be taken up by oblique-slip along favourably oriented pre-existing faults.

The fault pattern at different stages of the experiment provides important information on overall kinematics, stress field modifications and local partial partitioning of fault motion. The early fault style in transpression experiments clearly depends on the imposed ratio of shear strain rate and shortening strain rate. This ratio determines whether initial failure in brittle layers is accommodated by steep strike-slip faults (Riedel shears) or by thrust faults. In those experiments with a relatively high strain rate ratio (≥3.6) steep strike-slip faults (dipping at 80-90°) formed early. Their en-echelon arrangement can be used as a kinematic indicator for the shear component of transpression (i.e. a left-stepping pattern indicates dextral transpression; whereas a right-stepping pattern would indicate sinistral transpression). The surface strike orientations of the early Riedels (24-37°) are larger than in distributed shear experiments (Schreurs, 2003; 17-24°) and reflect the shortening component of deformation. Obliquity of surface strike of early Riedel shears increases for decreasing strain rate ratio. In low strain rate ratio experiments (≤2.7) pairs of thrust faults (dipping at 30-45°) initially form striking parallel to the longitudinal sidewalls of the model. These faults have opposite vergence and bound pop-up structures.

Older faults determine to a large extent the subsequent fault pattern and evolution, because they are favourably oriented for reactivation. Where strike-slip faults develop initially, further deformation creates several major anastomosing fault zones, consisting of steep oblique-slip faults along which the strike-slip component dominates. Positive flower structures are characteristic of such convergent strike-slip fault zones. The sigmoidal trace of strike-slip faults that laterally become oblique-slip reverse faults can be used as kinematic indicator for the overall sense of shear, i.e. a "lazy" Z-shape for dextral shear and a "lazy" S-shape for sinistral shear component (see also Mandl, 1988; Richard et al., 1995). In experiments where gently dipping reverse faults initially accommodate oblique deformation, an increase in strain leads to a fault pattern dominated by oblique-slip reverse faults.

Secondary faults forming in between earlier formed major fault zones reflect local stress field modifications that differ from the far-field stress system. Gently dipping reverse faults, striking very obliquely to the previously formed convergent strike-slip faults (experiment 1764), indicate that the maximum principal stress direction (s1) was locally reoriented sub-parallel to the major strike-slip fault zones. Partial partitioning of fault motion occurs late in experiments 1764, 1770 and 1820). Sub-vertical strike-slip faults generally formed late between or within pop-up structures. These strike-slip faults strike sub-parallel to oblique-slip reverse faults and are simultaneously active. The strike-slip faults usually merge at depth with oblique-slip reverse faults and generally have a curved fault trace ("lazy" Z-shape indicates a dextral shear and a "lazy" S-shape a sinistral shear component) and a dip direction which changes along strike. The close proximity of simultaneously active strike-slip faults and oblique-slip reverse faults indicates rapid lateral changes in the orientation of the principal stress axes.

There is good agreement between our experiments and natural examples of continental transpression (Schreurs & Colletta, 1998). Three-dimensional imaging of analogue models may provide constraints for geometric and kinematic interpretations of complex structures in natural zones of continental transpression.

Acknowledgments

Experiments were carried out at the Division Géologie-Géochimie of the Institut Français du Pétrole (Rueil Malmaison, France). Jean-Marie Mengus is thanked for technical assistance, and the scanner group for its help in obtaining the X-ray CT images. Research was funded by a grant from the Swiss National Science Foundation.

References

Anderson, E.M. 1951. The dynamics of faulting and dyke formation with applications to Britain. Oliver and Boyd, Edinburg.

Colletta, B., Roure, F., De Toni, B., Loureiro, D., Passalacqua, H. & Gou, Y. 1997. Tectonic inheritance, crustal architecture and contrasting structural styles in the Venezuela Andes. Tectonics. 16, 777-794.

Cunningham, D., Windley, B.F., Dorjnamjaa, D., Badamgarov, G. & Saandar, M. 1996. A structural transect across the Mongolian Western Altai: Active transpressional mountain building in central Asia. Tectonics, 15, 142-156.

England, P. 1989. Large rates of rotation in continental lithosphere undergoing distributed deformation. In: Kissel, C. & Laj, C. (eds). Paleomagnetic rotations and continental deformation, 157-164.

Hounsfield, G.N. 1973. Computerized transverse axial scanning (tomography). British Journal of Radiology, 46, 1016-1022.

Mandl, G. 1988. Mechanics of tectonic faulting. Amsterdam, Elsevier.

Molnar, P. & Taponnier, P. 1975. Cenozoic tectonics of Asia: effects of a continental collision. Science, 198, 419-426.

Mount, V.S. & Suppe, J. 1987. State of stress near the San Andreas fault: Implications for wrench tectonics. Geology, 15, 1143-1146.

Norris, R.J., Koons, P.O. & Cooper, A.F. 1990. The obliquely-convergent plate boundary in the South Island of New Zealand: implications for ancient collision zones. Journal of Structural Geology, 12, 715-725.

Richard, P.D., Naylor, M.A. & Koopman, A. 1995. Experimental models of strike-slip tectonics. Petroleum Geoscience, 1, 71-80.

Schreurs, G. 2003. Fault development and interaction in distributed strike-slip shear zones: an experimental approach. In: Storti, F., Holdsworth, R.E. and Salvini, F. (eds) : Intraplate strike-slip deformation belts. Geological Society, London, Special Publication, 210, 35-52.

Schreurs, G. & Colletta, B. 1998. Analogue modelling of faulting in zones of continental transpression and transtension. In: Holdsworth, R.E, Strachan, R.A. & Dewey, J.F. (eds.): Continental Transpressional and Transtensional Tectonics, Geological Society, London, Special Publication,135 59-79.

Weijermars, R. 1986. Flow behaviour and physical chemistry of bouncing putties and related polymers in view of tectonic laboratory applications. Tectonophysics, 124, 325-358.

Appendix 1 - Movies

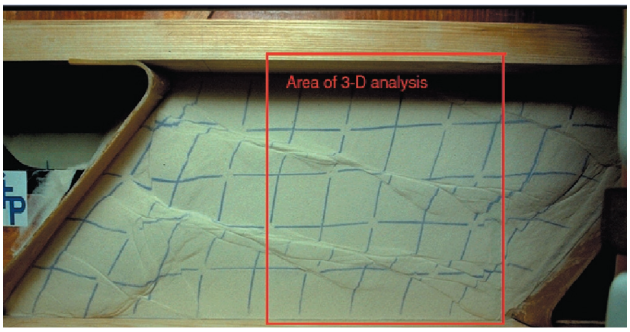

Movie 1661-01. Movie illustrating the progressive development of convergent strike-slip fault zones in plan view (experiment 1661). The first frame shows the location of computerized tomography (CT) acquisition planes. Rectangle in last frame indicates area of 3D analysis by X-ray CT (27 x 23.8 cm; see Movies 1661-03, 1661-04, 1661-05 and 1661-06). Initial grid spacing is 5 cm. Time between frames is about 10 minutes. **(Select image to view movie)**

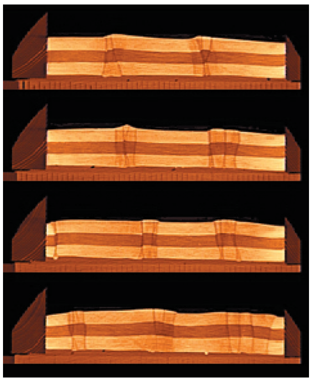

Movie 1661-02. Movie of cross-sectional evolution of experiment 1661. Location of CT sections A-D is given in the first frame of Movie 1661-01. Note that the position of the model changed with respect to the fixed CT image acquisition planes during progressive deformation. Initial width of model is 26 cm; initial height is 3.5 cm. Time between frames is 8 minutes. **(Select image to view movie)**

Movie 1661-03. Movie illustrating the geometry of convergent strike-slip fault zones by a series of serial vertical sections. Each of the 135 frames represents a 2mm thick cross-sectional CT slice. **(Select image to view movie)**

Movie 1661-04. Movie showing serial horizontal sections through convergent strike-slip fault zones. Major fault zones strike at about 15° to the longitudinal sidewalls. Horizontal sections were computed from 3D data set. First frame is near the base of the brittle layers. Vertical distance between frames is 0.5 mm. Computer animation shows 66 frames at three frames per second. **(Select image to view movie)**

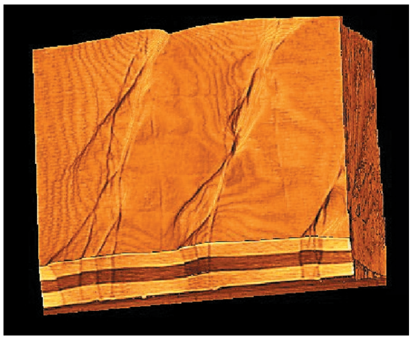

Movie 1661-05. Movie of rotating 3D perspective view of transpressional fault zones. Area of 3D CT analysis is indicated in Fig. 2E and in last frame of Movie 1661-01. **(Select image to view movie)**

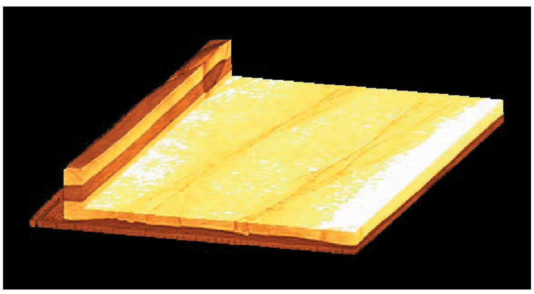

Movie 1661-06. Movie of cut-out 3D views of final deformation stage. Computer animation shows 28 frames at 4 frames per second. **(Select image to view movie)**

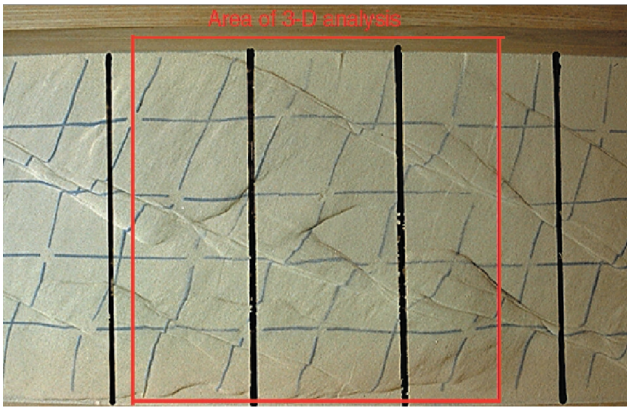

Movie 1764-01. Movie illustrating the progressive development of structures in plan view (experiment 1764). The first frame shows the location of CT acquisition planes. Rectangle in last frame indicates area of 3D analysis by X-ray CT (27 x 23.2 cm). Initial grid spacing is 5 cm. Time between frames is 10 minutes. **(Select image to view movie)**

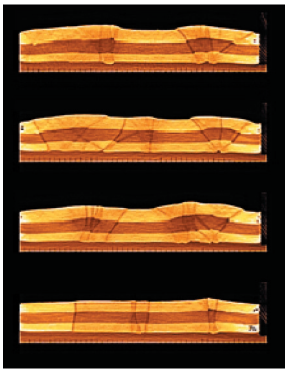

Movie 1764-02. Movie of cross-sectional evolution of experiment 1764. Location of CT sections A-D is given in the first frame of Movie 1764-01. Note the lateral changes in fault dip along strike. Initial width and height of model is 26 and 3.5 cm, respectively. Time between frames is 8 minutes. **(Select image to view movie)**

Movie 1764-03. Movie illustrating the fault geometry by a series of serial vertical sections. Steep strike-slip faults branch at depth with oblique-slip thrust faults. Each of the 135 frames represents a 2mm thick cross-sectional CT slice. **(Select image to view movie)**

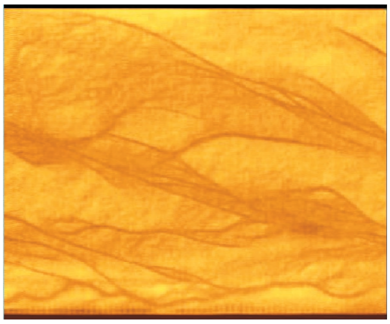

Movie 1764-04. Movie showing serial horizontal sections through final deformation stage. These sections show the complex fault pattern at depth in great detail. Note the oblique thrust faults (and associated vertical relief) between major convergent strike-slip fault zones in upper part of movie. First frame is near the base of the brittle layers. Vertical distance between frames is 0.5 mm. Computer animation consists of 64 frames. **(Select image to view movie)**

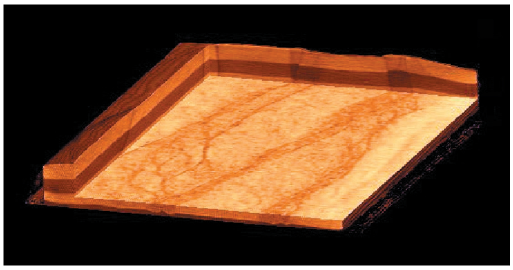

Movie 1764-05. Movie of cut-out 3D views of final deformation stage. Computer animation shows 28 frames at 4 frames per second. **(Select image to view movie)**

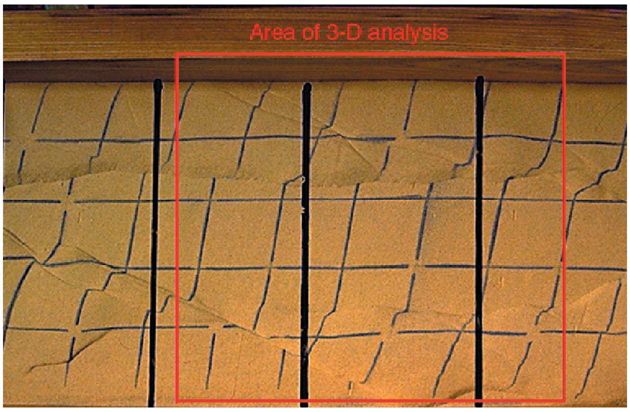

Movie 1820-01. Movie illustrating the progressive development of structures in plan view (experiment 1820). Main faults trend subparallel to longitudinal sidewalls. The first frame shows the location of CT acquisition planes. Rectangle in last frame indicates area of 3D CT analysis (27 x 22.7 cm). Initial grid spacing is 5 cm. Time between frames is 10 minutes. **(Select image to view movie)**

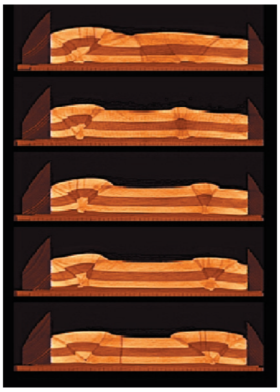

Movie 1820-02. Movie of cross-sectional evolution of experiment 1820. Pop-up structures form initially. Steep strike-slip faults form at later stages and occur either confined within pop-up structures or between different pop-up structures. Location of CT sections A-E is given in the first frame of Movie 1820-01. Initial width and height of model is 26 and 3.5 cm, respectively. Time between frames is 10 minutes.
(Select image to view movie)

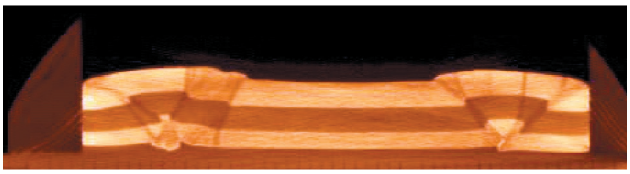

Movie 1820-03. Movie illustrating the fault geometry by a series of serial vertical sections. Fault dip changes along strike in the right-hand side of the images. Note also how subvertical strike-slip faults change their dip direction along strike and merge at depth with bounding thrust faults. Each of the 135 frames represents a 2mm thick cross-sectional CT slice. **(Select image to view movie)**

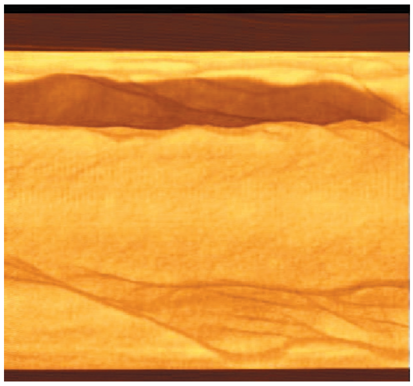

Movie 1820-04. Movie of serial horizontal sections through final deformation stage. Major faults are subparallel to the longitudinal borders of the model. First frame is near the base of the brittle layers. Vertical distance between frames is 0.5 mm. Computer animation consists of 60 frames. **(Select image to view movie)**

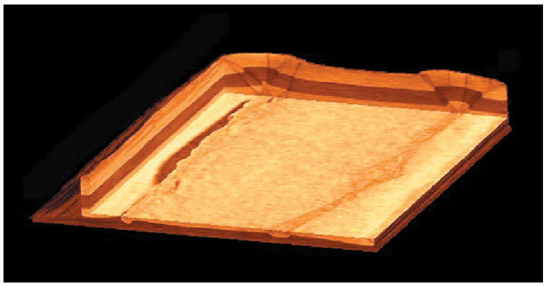

Movie 1820-05. Movie of cut-out 3D views of final deformation stage. Computer animation shows 28 frames at 4 frames per second.
(Select image to view movie)

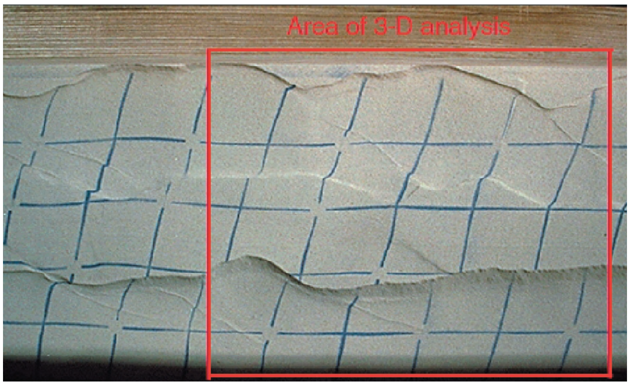

Movie 1770-01. Movie illustrating the progressive development of structures in plan view (experiment 1770). Main thrust faults trend parallel to longitudinal sidewalls. The first frame shows the location of CT acquisition planes. Rectangle in last frame indicates area of 3D CT analysis (27 x 22.7 cm). Initial grid spacing is 5 cm. Time between frames is 10 minutes. **(Select image to view movie)**

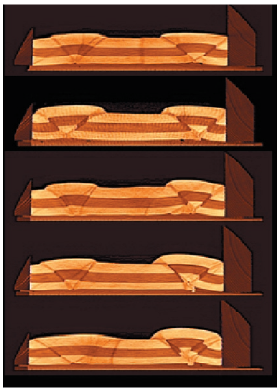

Movie 1770-02. Movie of cross-sectional evolution of experiment 1770. Model evolution dominated by thrust faulting. Location of CT sections A-E is given in the first frame of Movie 1770-01. Initial width and height of model is 26 and 3.5 cm, respectively. Time between frames is 10 minutes. **(Select image to view movie)**

Movie 1770-03. Movie illustrating the geometry of the structures by serial vertical sections. Subvertical strike-slip faults within pop-up structures change their dip direction along strike and merge at depth with bounding thrust faults. Each of the 135 frames represents a 2mm thick cross-sectional CT slice. **(Select image to view movie)**

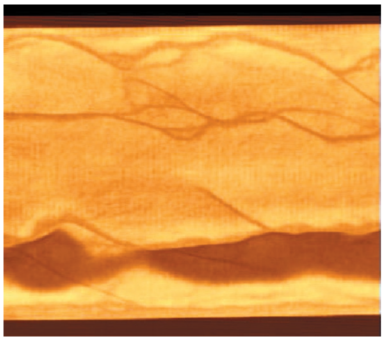

Movie 1770-04. Movie of serial horizontal sections through final deformation stage. Major faults are subparallel to the longitudinal borders of the model. Some strike-slip faults strike oblique to the longitudinal sidewalls. First frame is near the base of the brittle layers. Vertical distance between frames is 0.5 mm. Computer animation consists of 60 frames. **(Select image to view movie)**

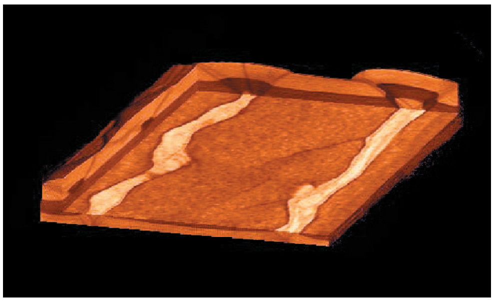

Movie 1770-05. Movie of cut-out 3D views of final deformation stage. Steep strike-slip faults within pop-up structures change their dip direction along strike. Computer animation shows 28 frames at 4 frames per second. **(Select image to view movie)**